Low-Level Updrafts in Stable Layers Forced by Convection

ISIDORO ORLANSKI AND BRUCE B. ROSS

Geophysical Fluid Dynamics Laboratory/NOAA, Princeton University, Princeton, NJ 08542

(Manuscript received 15 July 1985, in final form 19 December 1985)

ABSTRACT

An investigation is made of the stability of a convectively unstable atmosphere in the presence of a stably stratified layer beneath, which is moving with a constant velocity relative to the upper air. This work is an extension of the linear model presented as part of the recent study of Orlanski and Ross in which they sought to explain the structure of their simulated squall line. A stability analysis shows that two modes are possible: 1) the gravitational or convective mode due to the unstable stratification in the upper layer which modifies the stable region below and 2) the classical Kelvin–Helmholtz mode due to shear across the interface. The Kelvin–Helmholtz mode is of limited physical interest in this case. On the other hand, the gravitational mode produces an updraft structure similar to updrafts in the stable lower layer of a convective system. Analysis of the horizontal displacement of the surface convergence for this mode relative to the convergence in the convective zone shows this displacement to depend primarily on the wind, stratification, and depth of the stable lower layer. The resulting relationship provides a method for determining whether a dual or single updraft will occur in a convective system.

1. Introduction

As discussed in Orlanski and Ross (1984; hereafter referred to as OR), a major finding of Ogura and Liou (1980) was the existence of a strong midlevel convergence zone in the Oklahoma squall line of 22 May 1976 with this zone out of phase with the surface convergence. They attributed the divergence region beneath this midlevel feature to be the result of the effects of falling rain, namely, evaporative cooling and water loading. The numerical frontal solution of OR showed a very similar structure of intense midlevel convergence and low-level divergence which was out of phase with the surface convergence, i.e., the midlevel convergence maximum was displaced by a quarter wavelength to the rear of the low-level maximum within the squall line. (This displaced updraft structure between low and middle levels in the troposphere was referred to as a "dual updraft.") However, the numerical model used in their solution contained no rainwater phase and thus had no mechanism for evaporative cooling of rainwater beneath the cloud zone and only provided for water loading due to cloud water up to 1.5 gm kg^{-1}. This numerical result suggested that a simple dry model could explain the displacement of the surface convergence relative to the midlevel convergence zone in a hydrostatic convective system without the need for microphysics.

Hence, OR developed a simple, linear two-layer model to complement their full three-dimensional numerical simulation of a squall line. The linear model was shown to produce the basic dual updraft structure found in their moist simulation and in Ogura and Liou's (1980) observations. This model, which involves no moisture or microphysics, represents the cloud systems as two layers with a gravitationally unstable layer with zero wind above a stable lower layer with constant wind speed. The structure of the vertical motion fields in the lower layer, identified here as representing updraft–downdraft structures in the convectively stable lower layer of a convective system, were shown to depend on the low-level wind intensity, stratification, and layer depth for a given upper layer stratification and depth.

It is evident that this model will have two different unstable modes. First, a gravitational mode will be present due to the static instability of the upper layer. Second, a Kelvin–Helmholtz instability will occur due to the concentration of vorticity in the interface between the two layers.

In OR, only the gravitational mode was considered, being the only mode relevant to their discussion. This single mode solution came about because an incorrect interface condition was used, namely, that the vertical velocity rather than vertical displacement was continuous across the interface.[1] One purpose of this paper will be to investigate the full solution of the two-layer model and to determine the extent to which the gravitational mode is altered by the use of the displacement interface condition. In addition, a second important goal will be to use this two-layer model to identify what low-level conditions of wind and static stability will

[1] The authors thank Dr. Kerry Emanuel for pointing out the significance of using the correct condition of displacement continuity.

permit the formation of single-, dual-, and no-updraft in the low-levels of a convective system.

Section 2 will present a brief review of the two-layer model and a discussion of the full solution and the way in which the results of OR are modified. In section 3, an analysis is made of the more realistic gravitational mode which indicates how the structure of the low-level updraft depends upon conditions in the lower layer. Finally, section 4 will summarize these results.

2. Model solution

The two-layer model of OR, which will be briefly reviewed here, was formulated to represent the stable and unstable regions in a conditionally unstable atmosphere in which convection is occurring. The model atmosphere is assumed to be dry so as to avoid the complications of moist thermodynamics. In order to simulate the lifting of moist air to a level of free convection, the dry model environment is divided into two layers, each with constant stratification (Fig. 1). The lower layer is stably stratified ($\theta_{1z} > 0$) and extends from the surface to the level of free convection (LFC) at $z = h$. The upper layer is gravitationally unstable ($\theta_{2z} < 0$) to simulate the moist unstable cloud region above the LFC and extends to a rigid lid at $z = H$. The lower and upper layers are assumed to have constant mean winds U_1 and U_2, respectively, with the upper level wind U_2 set to zero.

A linearized inviscid two-dimensional form of the hydrostatic anelastic equations was assumed by OR to apply, namely:

$$\frac{\partial u'}{\partial t} + U_m \frac{\partial u'}{\partial x} = -c_p \Theta \frac{\partial \pi'}{\partial x}, \tag{2.1}$$

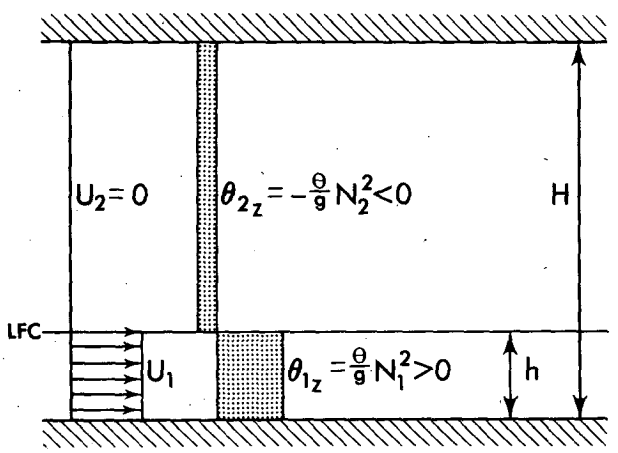

FIG. 1. Schematic diagram showing the configuration of the simple dry model containing two layers, each with constant stratification (indicated schematically by the stippled bars) and uniform winds. (The upper-layer wind, U_2, is assumed to be zero.) The interface between the two layers is viewed as representing the level of free convection (LFC) in the moist environment being modeled.

$$\frac{\partial \theta'}{\partial t} + U_m \frac{\partial \theta'}{\partial x} + w' \theta_{m_z} = 0, \tag{2.2}$$

$$0 = -c_p \Theta \frac{\partial \pi'}{\partial z} + \frac{g}{\Theta} \theta', \tag{2.3}$$

$$\frac{\partial u'}{\partial x} + \frac{\partial w'}{\partial z} = 0, \tag{2.4}$$

where subscript m refers to layers 1 and 2, density variations have been neglected, and primes denote perturbation quantities.

a. The eigenvalues

A streamfunction Φ' may be defined to satisfy the continuity equation (2.4). Then, if all perturbation quantities are assumed to vary as $\exp[ik(x - ct)]$ so that $\Phi' = \Phi(z) \exp[ik(x - ct)]$, we obtain the following equations by combining (2.1)–(2.3):

$$\frac{\partial^2 \Phi_1}{\partial z^2} + \frac{N_1^2}{(U_1 - c)^2} \Phi_1 = 0 \quad \text{(lower layer)}, \tag{2.5a}$$

$$\frac{\partial^2 \Phi_2}{\partial z^2} - \frac{N_2^2}{c^2} \Phi_2 = 0 \quad \text{(upper layer)}, \tag{2.5b}$$

where we have used the fact that $U_2 = 0$ and have defined the positive quantities N_1^2 and N_2^2 such that $N_1^2 = g\theta_{1z}/\Theta$ and $N_2^2 = -g\theta_{2z}/\Theta$. Conditions at the rigid boundaries are

$$\Phi = 0 \quad \text{at} \quad z = 0, H. \tag{2.6}$$

The following conditions will be used here for the interface, $z = h$:

$$\frac{\Phi_1(h)}{U_1 - c} = -\frac{\Phi_2(h)}{c} \quad \text{(continuity of displacement)}, \tag{2.7a}$$

and

$$(U_1 - c)\Phi_{1z}(h) = -c\Phi_{2z}(h) \quad \text{(continuity of } \pi'\text{)}. \tag{2.7b}$$

Note that the condition, (2.7a), differs from the condition of continuity of w' which was used by OR [their Eq. (4.7a)], namely,

$$\Phi_1(h) = \Phi_2(h). \tag{2.7a'}$$

The general solution of (2.5) which satisfies the boundary conditions (2.6) is

$$\Phi_1 = \hat{\Phi}_1 \sin\gamma_1 z \quad \text{(lower layer)}, \tag{2.8a}$$

$$\Phi_2 = \hat{\Phi}_2 \sinh\gamma_2 (H - z) \quad \text{(upper layer)}, \tag{2.8b}$$

where γ_1 and γ_2 are complex wave numbers of the form

$$\gamma_1 = \gamma_{1_r} + i\gamma_{1_i}$$

$$= \pm \frac{N_1 c_r}{(U_1 - c_r)^2 + c_i^2} \pm i \frac{c_i N_1}{(U_1 - c_r)^2 + c_i^2}, \tag{2.9a}$$

$$\gamma_2 = \gamma_{2r} + i\gamma_{2i} = \mp \frac{N_2 c_r}{c_r^2 + c_i^2} \pm i \frac{c_i N_2}{c_r^2 + c_i^2}, \quad (2.9b)$$

with $i = (-1)^{1/2}$. Only the upper sign in the above expressions will be used hereafter.

Finally, the requirement that (2.8) satisfy the interface conditions, (2.7), produces the transcendental equation

$$\tanh\gamma_2(H - h) = \frac{c}{U_1 - c} \frac{N_2}{N_1} \tan\gamma_1 h \quad (2.10)$$

which must be solved to determine the complex eigenvalue, $c_r + ic_i$, for the eigenfunction (2.8).

As has been discussed in OR, the parameters controlling the solution of the two-layer model are the low-level wind, U_1, the ratio of static stabilities, $P \equiv N_1/N_2$, and the ratio of the depths of the lower and upper layers, $\epsilon \equiv h/(H - h)$. As in OR, solutions of the two-layer model have been obtained here by using a two-dimensional Newton–Raphson technique (see Hamming, 1962, p. 357) to determine the complex eigenvalues c of (2.10). The complete solution for the growth rate, c_i, and the phase speed, c_r, as a function of low-level wind, U_1, is shown in Figs. 2a and 2b. In these figures, the gravitational or convective and Kelvin–Helmholtz solutions are designated by the letters G and KH, respectively. The two numbers in parentheses after the letter designations indicate, in order, the static stability ratio, P, and the height ratio, ϵ. The P values used are 1, 10, and 30, while values of ϵ are 0.1 and 1.

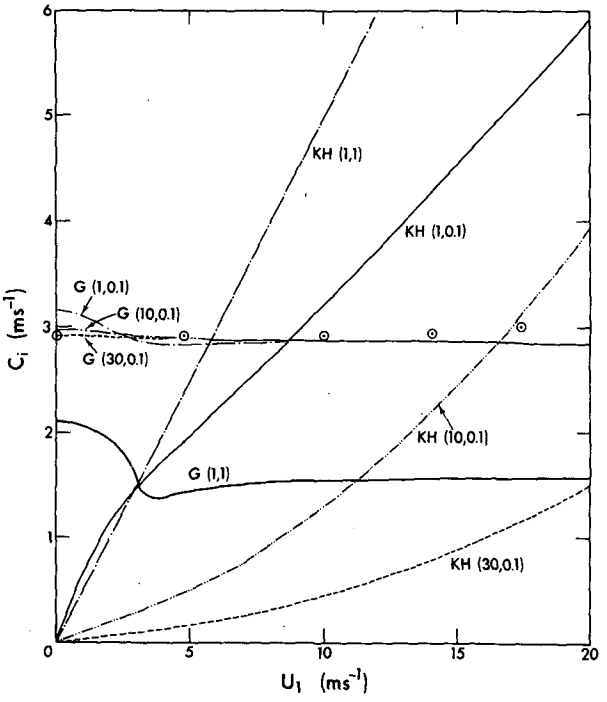

FIG. 2a. Plot of imaginary eigenvalue c_i, in m s^{-1}, as a function of wind U_1 in the lower layer for different values of stability ratio, P, and height ratio, ϵ. Kelvin–Helmholtz and gravity wave modes are indicated by "KH" and "G" respectively. The two numbers in brackets following the mode designation indicate the corresponding values of P and ϵ. The circle symbol indicates values for the case G(30, 0.1) from OR.

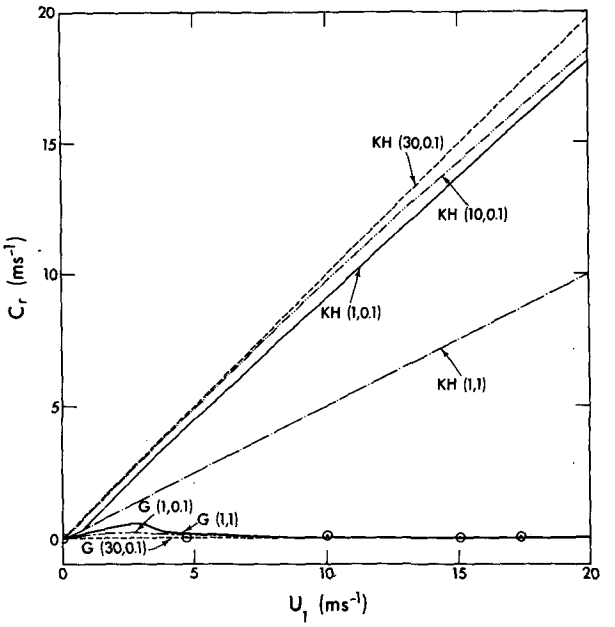

FIG. 2b. As in Fig. 2a but for real eigenvalue c_r.

Characteristics of the growth rate c_i are distinctly different for the two different kinds of modes. The Kelvin–Helmholtz value of c_i is seen to be roughly proportional to U_1 for all values of P used. (Note that U_1 represents the shear between layers, because the wind, U_2, of the upper layer is zero.) On the other hand, the growth rate of the gravitational mode is quite invariant with wind U_1 and hence with shear across the interface. In fact, the value of c_i of approximately 3 m s^{-1} found for $\epsilon = 0.1$ and for the three different values of P is effectively determined by the growth rate, $N_2(H - h)/\pi$, which is the value for a single layer of thickness $H - h$ and unstable stratification of magnitude N_2. [This is the unstable mode found by Kuo (1963).][2] Because of the insensitivity of the gravitational mode to shear at the interface, the solution of OR for $P = 30$ and $\epsilon = 0.1$ (indicated by a circle in Figs. 2a, b) is very similar to that found using the corrected interface condition.

The only major difference among the G modes shown is for the case G(1, 1). However, this mode still

[2] Although values for the layer thicknesses h and $H - h$ can be obtained from observations in a straightforward manner, it is difficult to directly determine a value for the unstable stratification which prescribes N_2. However, one may obtain a rough estimate of the growth rate, c_i, from the ratio between the horizontal scale of the convective system and the time scale of the instability. For example, the assumed value for c_i of 3 m s^{-1} might correspond to a horizontal scale of 100 km and a time scale of 9 hours. For an unstable layer thickness, $H - h$, of 9000 m as used here, this value of c_i implies a magnitude for N_2 of 10^{-3} s^{-1}.

exhibits similarities to the others in that the maximum instability occurs for zero shear, while the growth rate is smaller and nearly constant for high shear. The limiting value for this mode for large U_1 will be $N_2H/(2\pi)$, implying that the growth rate for $\epsilon = 1$ will be roughly half that for $\epsilon = 0.1$.

Figure 2a shows the expected tendency for c_i to increase with increasing shear for the Kelvin–Helmholtz (KH) modes (Emanuel, private communication, 1984).[3] In particular, note that the mode, KH(1, 1), is a straight line in the figure with a slope of 0.5. Finally, note that the Kelvin–Helmholtz instability decreases as the stratification ratio, P, increases.

Figure 2b shows the phase speed, c_r, of the KH modes also to be proportional to U_1 with the mode KH(1, 1) described by $c_r = U_1/2$. Comparison of the two modes, KH(1, 1) and KH(1, 0.1), shows that the phase speed increases as the depth of the lower layer decreases.[4]

The phase speed for the gravity mode is shown in Fig. 2b to be nearly zero and is insensitive to the low-level wind, U_1. This phase speed will be determined by the mean velocity, U_2, of the convective disturbance in the upper level which is zero in this case. Because of this strong dependence on the upper level wind, good agreement was found between the approximate solution of OR (indicated in Fig. 2 by a circle) and the results presented here. This agreement will be explained in more detail in the following discussion.

b. *Structure of the unstable modes*

Figure 3 shows a comparison of vertical velocity fields for the two different unstable modes, the gravitational and the Kelvin–Helmholtz, for the parameter values, $P = 10$, $U_1 = 5$, and $\epsilon = 0.1$. The main characteristic of the gravitational or convective mode is a maximum disturbance in the center of the convectively unstable upper layer with only a weak influence on the stable lower layer. In fact, the figure shows vertical velocity to be very small at the interface and inside the lower layer. The Kelvin–Helmholtz mode is quite different in this regard, since the vertical velocity disturbance is maximum at the interface with strong penetration into the unstable layer and weaker penetration into the stable layer.

One of our primary interests here is the position of the surface convergence relative to the location of the maximum convergence of the wave, particularly for the gravitational or convective mode. Figure 4 shows a comparison of the nondimensional convergence, $w_z h/w_{\max}$, for the two different modes. Note that, for the gravity wave mode, the convergence amplitude at the surface is comparable to the maximum at the interface. For the Kelvin–Helmholtz mode, on the other hand, the maximum convergence at the interface decays very rapidly below the interface with insignificant convergence in the stable layer.

In view of the foregoing considerations, it now is easy to explain the close similarity between the eigen-

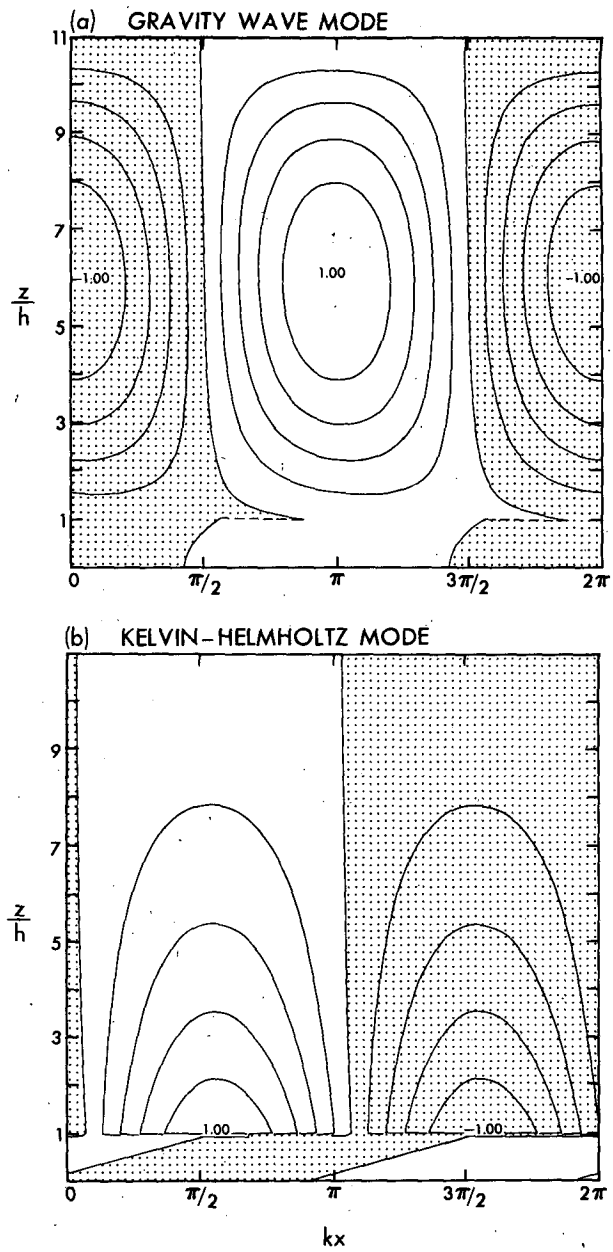

FIG. 3. Contour plots, over one wavelength, of the distribution of normalized vertical velocity, $w/w_{\max}$, for (a) the gravity wave and (b) Kelvin–Helmholtz modes with $P = 10$, $U_1 = 5$ m s^{-1}, and $\epsilon = 0.1$.

[3] Emanuel has obtained a particular solution, $c_r = c_i = U_1/2$, for this case $P = \epsilon = 1$, which is verified by these results.

[4] One can derive an expression for c_r and c_i in the analogous unstratified, but nonhydrostatic case with $N_1 = N_2 = 0$:

$$c_r = \frac{U_1 \tanh k(H-h)}{\tanh kh + \tanh k(H-h)}, \quad c_i = \pm \frac{U_1[\tanh kh \tanh k(H-h)]^{1/2}}{\tanh kH + \tanh k(H-h)}.$$

This expression shows that, in the limit $h \to 0$, then $c_r \to U_1$ and $c_i \to 0$, in agreement with the above behavior.

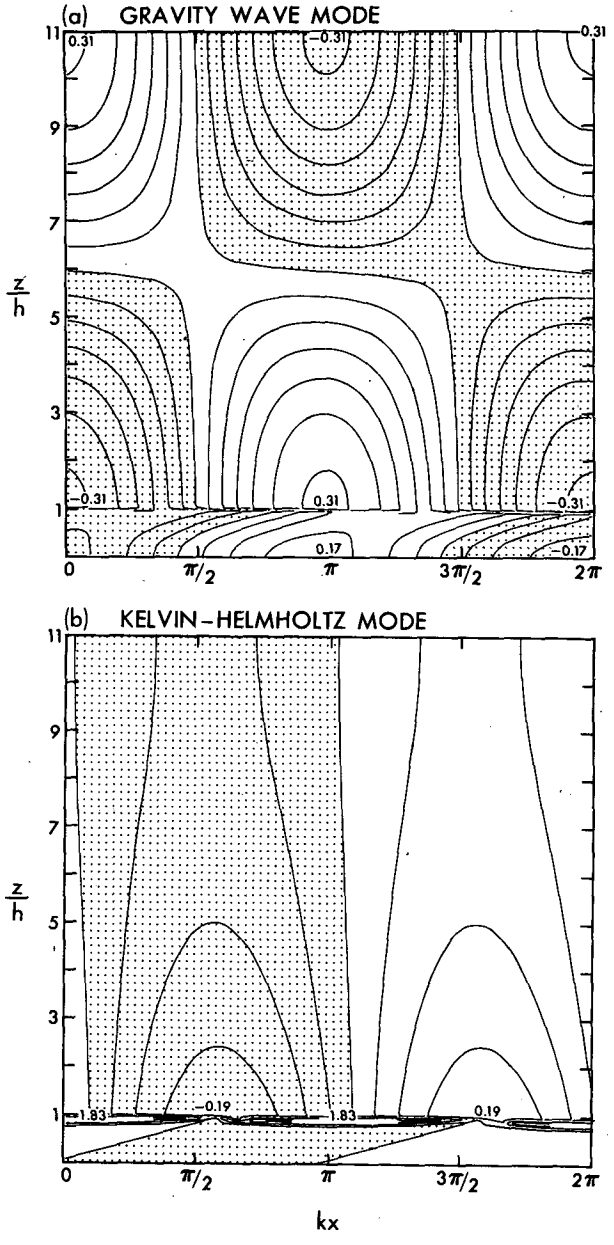

FIG. 4. Contour plots, over one wavelength, of the distribution of normalized horizontal convergence, $w_z(h/w_{max})$, for (a) the gravity wave and (b) Kelvin–Helmholtz modes as in Fig. 3.

values for the gravity-wave mode (Fig. 2) of OR's approximate solution and the exact solution. The fundamental difference between these two solutions is the use of the interface condition of w continuity, (2.7a'), in the former versus displacement continuity, (2.7a), in the latter. However, as Fig. 3 indicates, vertical velocity (as well as displacement) is very small at the interface for the gravity wave mode. In this case, the pressure continuity condition, (2.7b), which is the same in both OR's and the present solution, is the most important interface condition as indicated by the magnitude of w_z at $z = h$ in the upper frame of Fig. 4a. As a result, both the eigenvalues and the structure of the eigenmodes will be nearly identical in each case.

Figure 5 shows the distribution of vertical velocity and horizontal convergence for $P = 30$, $U_1 = 4.75$ m s^{-1}, and $\epsilon = 0.1$. Comparison of this with Fig. 22 of OR, in which the same parameter values were used, shows very similar structures. Note that slight discontinuities are evident in w at $z = h$, since vertical velocity is no longer continuous at the interface. As before, the surface convergence is displaced by an amount $\phi = \pi$

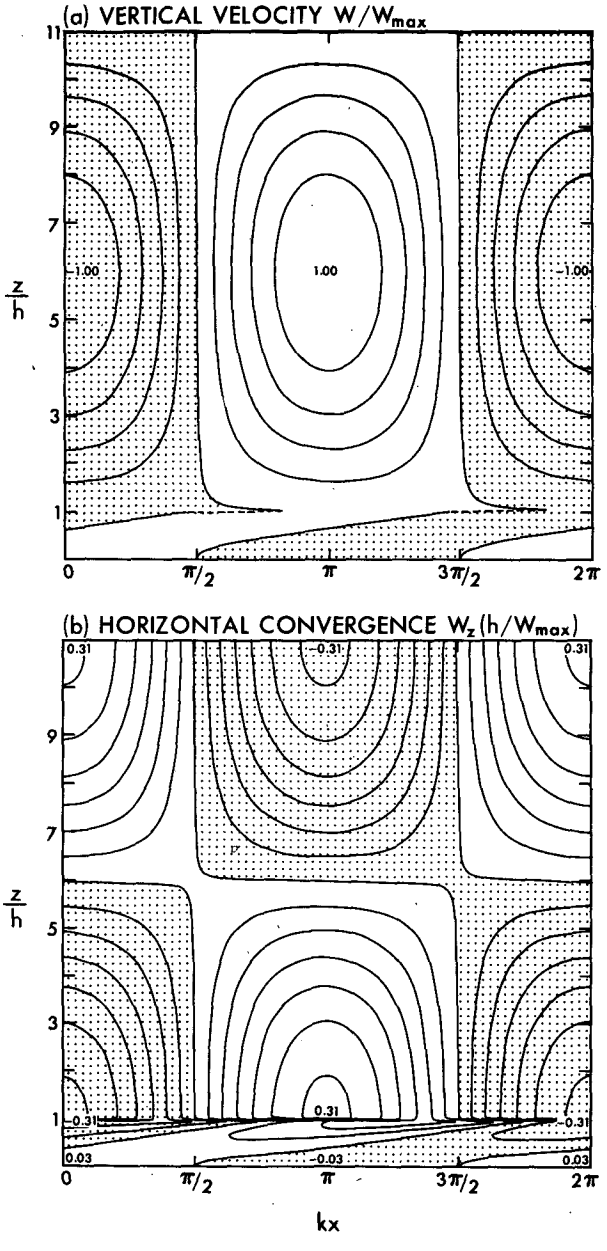

FIG. 5. Contour plots of distribution of (a) vertical velocity and (b) horizontal convergence corresponding to low-wind case ($U_1 = 4.75$ m s^{-1}, $P = 30$, $\epsilon = 0.1$) shown in Fig. 22 of OR.

upstream of the interface maximum for these values of P and U_1. Note also, that, although low-level wind, U_1, is similar to that of Fig. 4a (4.75 versus 5 m s^{-1}), the low-level structure is quite different owing to its strong dependence on the stratification of the lower layer with $P = 30$ here and $P = 10$ for Fig. 4. The dependence of the phase shift, ϕ, upon flow parameters will be investigated in section 3.

3. Structure of the low-level updraft

As previously discussed, the structure of the gravitational unstable mode in the stably stratified region depends upon the wind speed, U_1, the depth of the layer, h, and its stratification, N_1. A fundamental characteristic of the solutions in this lower level, as exhibited by the structure of vertical velocity and divergence in Figs. 3 and 4, is the tendency for convergence at the surface to be displaced either upstream or downstream relative to the convergence maximum at the interface level, $z = h$. In the present section, a more detailed analysis will be made of the phase angle difference between the surface and interface convergence maxima as a function of U_1, N_1, and h. Derivation of this phase shift will be done in a straightforward manner using the interface condition for pressure continuity, (2.7b), namely,

$$(U_1 - c)\Phi_{1_z}(h) = -c\Phi_{2_z}(h) \tag{3.1}$$

where

$$\Phi_{1_z}(z) = \gamma_1\hat{\Phi}_1 \cos\gamma_1 z \tag{3.2}$$

as obtained by differentiating (2.8a) with respect to z. Values of Φ_{1_z} in the lower layer at $z = 0$ and $z = h$ are then determined from (3.2) to be, respectively,

$$\Phi_{1_z}(0) = \gamma_1\hat{\Phi}_1, \tag{3.3a}$$

$$\Phi_{1_z}(h) = \gamma_1\hat{\Phi}_1 \cos\gamma_1 h, \tag{3.3b}$$

so that (3.1) may be expressed in terms of $\Phi_{1_z}(0)$, using (3.3), as

$$\Phi_{1_z}(0) = -\frac{c}{U_1 - c\cos\gamma_1 h}\frac{1}{\Phi_{2z}(h)}. \tag{3.4}$$

Since we are interested only in the gravity mode, we may assume that $c_i \approx N_2(H-h)/\pi$ and $c_r \approx 0$ to a good approximation. Then the expression, (2.9a), for vertical wave number, $\gamma_1 \equiv \gamma_{1_r} + i\gamma_{1_i}$, becomes

$$\gamma_{1_r} = \frac{N_1 U_1}{U_1^2 + c_i^2}, \quad \gamma_{1_i} = \frac{N_1 c_i}{U_1^2 + c_i^2}$$

or, using nondimensional parameters on the right-hand side:

$$\gamma_{1_r}h = \frac{\mathcal{U}}{\mathcal{U}^2 + 1}\pi P\epsilon, \tag{3.5a}$$

$$\gamma_{1_i}h = \frac{1}{\mathcal{U}^2 + 1}\pi P\epsilon \tag{3.5b}$$

where $\mathcal{U} \equiv U_1/c_i$, $P \equiv N_1/N_2$, $\epsilon = h/(H-h)$. By manipulating the algebra of the real and imaginary parts, we can write (3.4) as

$$\Phi_{1_z}(0) = \frac{-i\Phi_{2_z}(h)(\mathcal{U} + i)\cos(\gamma_{1_r}h - i\gamma_{1_i}h)}{(\mathcal{U}^2 + 1)|\cos(\gamma_{1_r}h + i\gamma_{1_i}h)|^2} \tag{3.6}$$

or, in reduced form,

$$\Phi_{1_z}(0) = \Phi_{2_z}(h)\mathcal{A}e^{i\phi}$$

where $\Phi_{2_z}(h)\mathcal{A}$ is the real, positive amplitude of the right-hand side of (3.6) and ϕ is the phase shift between convergence maxima at $z = h$ and $z = 0$. This phase angle takes the form

$$\phi = \arctan\left[\frac{\tan\gamma_{1_r}h\tanh\gamma_{1_i}h - \mathcal{U}}{1 + \mathcal{U}\tan\gamma_{1_r}h\tanh\gamma_{1_i}h}\right] \tag{3.7}$$

where $\gamma_{1_r}h$ and $\gamma_{1_i}h$ are given by (3.5) in terms of $\mathcal{U}$ and $P\epsilon$.

Figure 6 shows a plot of curves of constant ϕ as a function of $\mathcal{U}$ and $P\epsilon$. Values of $P\epsilon$ considered in section 2 generally range from one to three for $\epsilon = 0.1$. For this range of $P\epsilon$ and for large $\mathcal{U}$, the phase ϕ is negative, implying that low-level divergence occurs upwind of the convective cell and low-level convergence occurs downwind. As the wind, $\mathcal{U}$, decreases, the phase increases to zero, corresponding to a vertical structure with surface convergence directly beneath the cloud convergence. We will refer to this configuration as a single updraft. Further decrease of $\mathcal{U}$ produces a positive phase ϕ, which means the surface convergence is

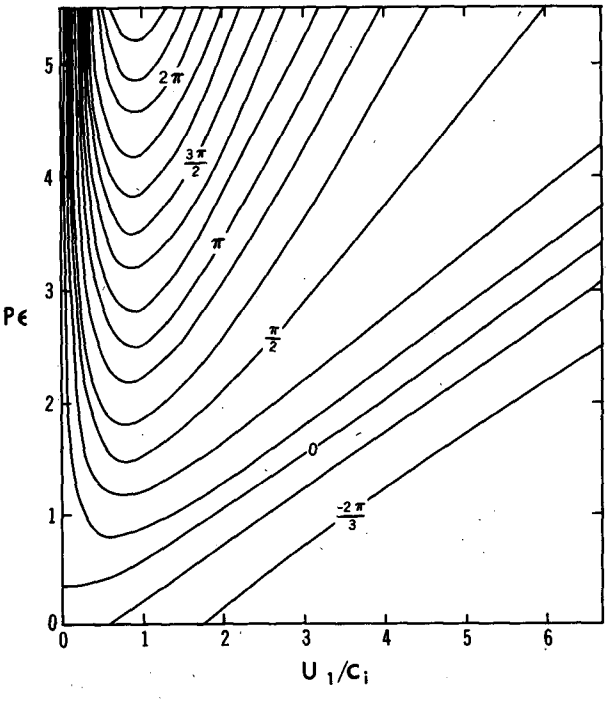

FIG. 6. Plot of contours of phase shift between the surface convergence maximum and the maximum above $z = h$ for nondimensionalized parameters $P\epsilon$ and U_1/c_i, as obtained from Eq. (3.7).

upwind and surface divergence downwind relative to the cloud convergence. When the phase ϕ reaches π, surface convergence will be exactly out of phase with cloud convergence (i.e., surface divergence is located directly beneath the cloud convergence). This structure represents what we refer to here as a dual updraft. Note that the increase in the phase shift found here implies an increase in the vertical wave number of the gravity wave structure in the stable lower layer. This will be discussed further in what follows. Finally, as the wind approaches zero, the phase ϕ reaches a maximum and then decreases rapidly back to zero. This limit represents the required condition that the updraft have no tilt in the zero-wind case.

It is clear from this analysis that some updraft structures predicted by the two-layer model will be unrealizable in nature or at least will not persist in a long-lived convective system. In particular, the cases with negative phase cannot be maintained in a real convective system, because the positioning of low-level divergence upstream of the cloud will interfere with the supply of low-level moisture to the convective updraft. Likewise, cases with phases larger than π (upper left portion of Fig. 6) are not realistic, because they would imply that surface convergence is overly remote (several horizontal cloud scales) from the convective zone of the cloud. The above discussion thus suggests that realistic configurations, i.e., those permitting an adequate supply of low-level moisture to reach the cloud, must have a phase angle lying in the approximate range between zero and π.

The structure of the waves in the stably stratified layer can be interpreted as being that of an unstable wave which is forced at the interface by the convection above. Also, both the horizontal wave length and the phase speed of this wave must match those of the convectively unstable wave in the upper layer. Then since the wind speed, U_2, and hence the phase speed in the upper layer are zero, the phase speed of the wave in the lower layer must match this wind speed so that the net propagation speed, c_r, is zero. Since horizontal wave number and phase speed are prescribed by the unstable convective cell in the upper layer, only the complex vertical wave number remains to be specified by the dispersion relation (which should be analogous to that of a neutral gravity wave in the stable lower layer). This relation, in turn, depends on the conditions across the interface. Reference to the vertical structure of $\Phi(z)$ near the interface indicates that Φ_z will be large, while Φ will be quite small for the gravity or convective mode of interest here. Hence pressure continuity, (2.7b), rather than displacement continuity, (2.7a), will be the controlling condition for the dispersion relation, as discussed earlier.

Finally it should be noted that the solutions obtained will simply be inverted if the stably stratified layer is relocated above rather than below the convective layer. Hence Fig. 6 will also describe the phase shift of internal gravity waves forced by the penetration of convectively unstable cells into a stable layer above them. In this configuration, there is no physical restriction on the phase angle since all waves are now possible. Of course, the assumption of a rigid lid located above the stable layer is unrealistic. However, the disturbance will decay exponentially above the interface; for this reason, the lid assumption may not be such a bad approximation.

4. Summary

The stability analysis of the two-layer configuration given herein, with one layer stable and the other unstable and with relative motion between them, has shown that two modes are possible: 1) the classical Kelvin–Helmholtz mode due to shear at the interface and 2) the gravitational or convective mode due to the unstable stratification in the one layer which also modifies the stable layer adjacent to it. The behavior of the Kelvin–Helmholtz mode is well known. The phase speed and growth rate are proportional, respectively, to the average wind speed and the shear across the interface. (In the present discussion, both wind and shear are determined by U_1.) As expected, an increase in the stratification of the lower layer reduces the growth rate of the mode. The phase speed tends to be proportional to a depth-weighted average velocity of the two layers. Hence, when the layers have equal thickness, c_r will be $U_1/2$ if the magnitudes of the stratification in each layer are equal. A more peculiar result, evident in Fig. 2, is that c_r tends to U_1 as the layer thickness, h, of the stable layer goes to zero. (This result is consistent with the analytic solutions for the special case of zero stratification in both layers.)

Our main interest in this paper concerns the structure of the convective mode. Hence, because the Kelvin–Helmholtz mode occurs due to the artificiality of the two-layer model, we have not elaborated much on this mode. However, for models with more realistic, continuous wind profiles, this mode will be of interest in relation to the convection itself.

The growth rate of the gravitationally unstable or convective mode was found to be insensitive to the wind speed and stratification of the stable layer. In fact, the growth rate for all cases was proportional to the product of the unstable stratification, N_2, and the depth of the unstable layer, $H - h$, as one might expect.

On the other hand, the structure of the stable layer which is compatible with the convective cell depends on the stratification, depth, and wind speed of the stable layer. This is the case because the convective cell excites a gravity wave in this stable layer which must match the phase speed of the unstable cell. For a given stable layer stratification and depth, a multitude of possible solutions exist which depend upon the wind speed, U_1; however, many of these solutions are not realizable in a moist convective atmosphere, because they would prevent moisture from the surface layer (the bottom

of the stable layer in this model) from reaching and maintaining the convective cell. Because of this selectivity, only a few configurations are capable of sustaining moist convection.

Figure 7, which is a dimensional, schematic representation of Fig. 6, indicates the possible low-level updraft configurations which will result for different low-level wind speeds. In Fig. 6, the nondimensional quantities, $\mathcal{U}$ and $P\epsilon$, were used, respectively, for the abscissa and ordinate. However, the crucial parameter for nondimensionalizing U_1 in $\mathcal{U}$ is the growth rate, c_i, of the convective cell. This was shown above to depend only on the characteristics of the unstable layer. For the primary cases considered in section 2 ($\epsilon = 0.1$), c_i was approximately 3 m s^{-1}, independent of N_1 and U_1. This growth rate, which was somewhat arbitrary, would imply that a storm with a 10-km width would have a growth time scale of roughly an hour. Similarly, for a squall line with a 100-km width, the time scale would be the order of a half day, which is also fairly realistic. Hence, for the results shown in Fig. 7, we have chosen to use this value of 3 m s^{-1} for c_i.

Different regions of the graph in Fig. 7 are indicated by stippling, hatching, and cross-hatching to indicate the different structures of the low-level updraft. In particular, the stippled zones in the figure indicate those parameter values for which the updraft structure is sloped away from the low-level wind and is unable to carry surface moisture up to the convective cell. Hence, the only physically viable updraft configurations occur for phase angles between roughly 0° and 180°. The single and dual updraft ranges are indicated by cross-hatching and hatching, respectively. The schematic drawings on the right side of Fig. 7 illustrate the primary configurations.

Included in Fig. 7 are data points for the observed squall line of Ogura and Liou (1980), indicated by boxes, and the simulated squall line of OR, designated by circles. The growth rate, c_i, has been estimated from the horizontal storm scale divided by the time which the convective system takes to grow to maturity. In both systems, the horizontal scale is assumed to be 150 km. However, the time scale is difficult to determine; accordingly, a range between 6 and 12 hours has been displayed in the figure with the corresponding hour indicated within each symbol. These data ranges indicate changes required due to differences in the actual value of c_i as compared to the value of 3 m s^{-1} which

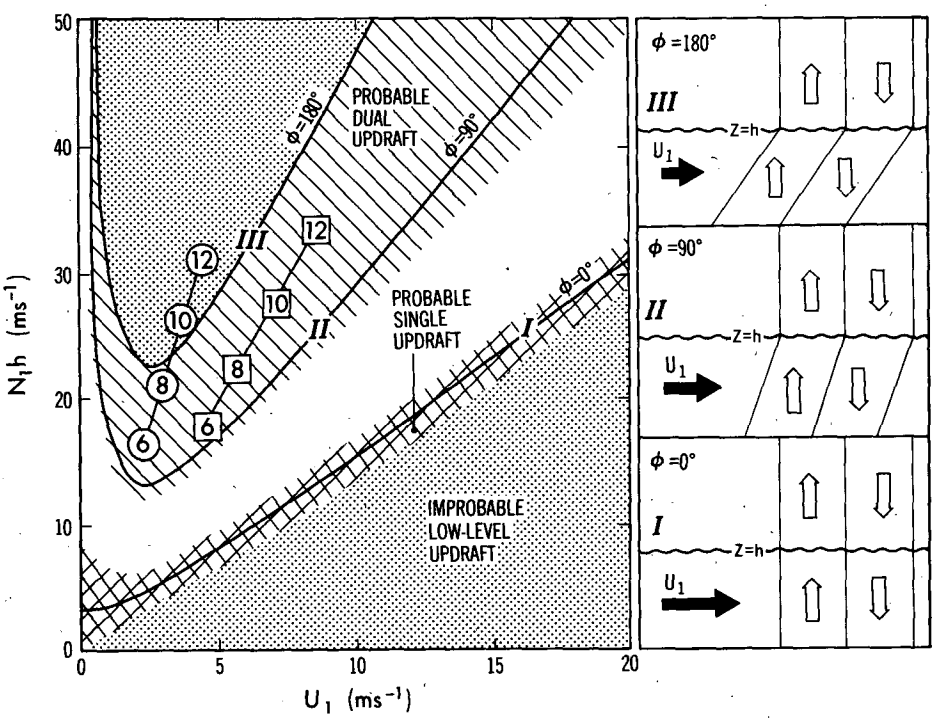

FIG. 7. Schematic diagram summarizing dependence of phase shift, ϕ, on low-level wind, U_1, and the product of stratification, N_1, and depth, h, of the stable lower layer for $c_i = 3$ m s^{-1}. Cross-hatching indicates the range of probable single updraft; hatching indicates probable dual updraft; and stippling designates parameter ranges for which low-level updrafts are unlikely to occur in nature. [See text for a discussion of data points corresponding to the observed squall line of Ogura and Liou (1980) (box symbols) and the simulated squall line of OR (circle symbols).] Diagrams on the right show the structure of the updraft–downdraft system for cases with phase shifts of 0°, 90°, and 180° with the Roman numerals I, II, and III on the curves corresponding to those in the diagrams.

was used to convert Fig. 6 to the dimensional form shown here. (A time scale of 14 hours corresponds to a c_i of 3 m s^{-1}.) Both sets of data points tend to fall within the dual updraft range, except for the estimates for the simulation involving longer time scales. One should treat this rather remarkable agreement with considerable caution in view of the roughness of the estimates involved and the fact that we are applying results from a linear model to finite-amplitude systems.

Finally, note that while these solutions are adiabatic, they indicate possible states of the convective system wherein diabatic effects, such as evaporative cooling beneath the cloud due to rainfall, may enhance and maintain the structure of the updraft.

Acknowledgments. The authors thank Dr. Kerry Emanuel for suggesting the proper interface condition to be used in the linear model. They also thank Dr. Frank Lipps for his help in clarifying the manuscript. Finally, their appreciation is expressed for the excellent work of Mrs. Joan Pege in typing the manuscript and Messrs. John Connor and Phil Tunison and other members of the GFDL drafting group in preparing the figures.

REFERENCES

Hamming, R., 1962: *Numerical Methods for Scientists and Engineers,* McGraw-Hill, 411 pp.

Kuo, H. L., 1963: Perturbations of a plane Couette flow in stratified fluid and origin of cloud streets. *Phys. Fluids,* **6,** 195–211.

Ogura, Y., and M. T. Liou, 1980: The structure of a midlatitude squall line: A case study. *J. Atmos. Sci.,* **37,** 553–567.

Orlanski, I., and B. B. Ross, 1984: The evolution of an observed cold front. Part II: Mesoscale dynamics. *J. Atmos. Sci.,* **41,** 1669–1703.